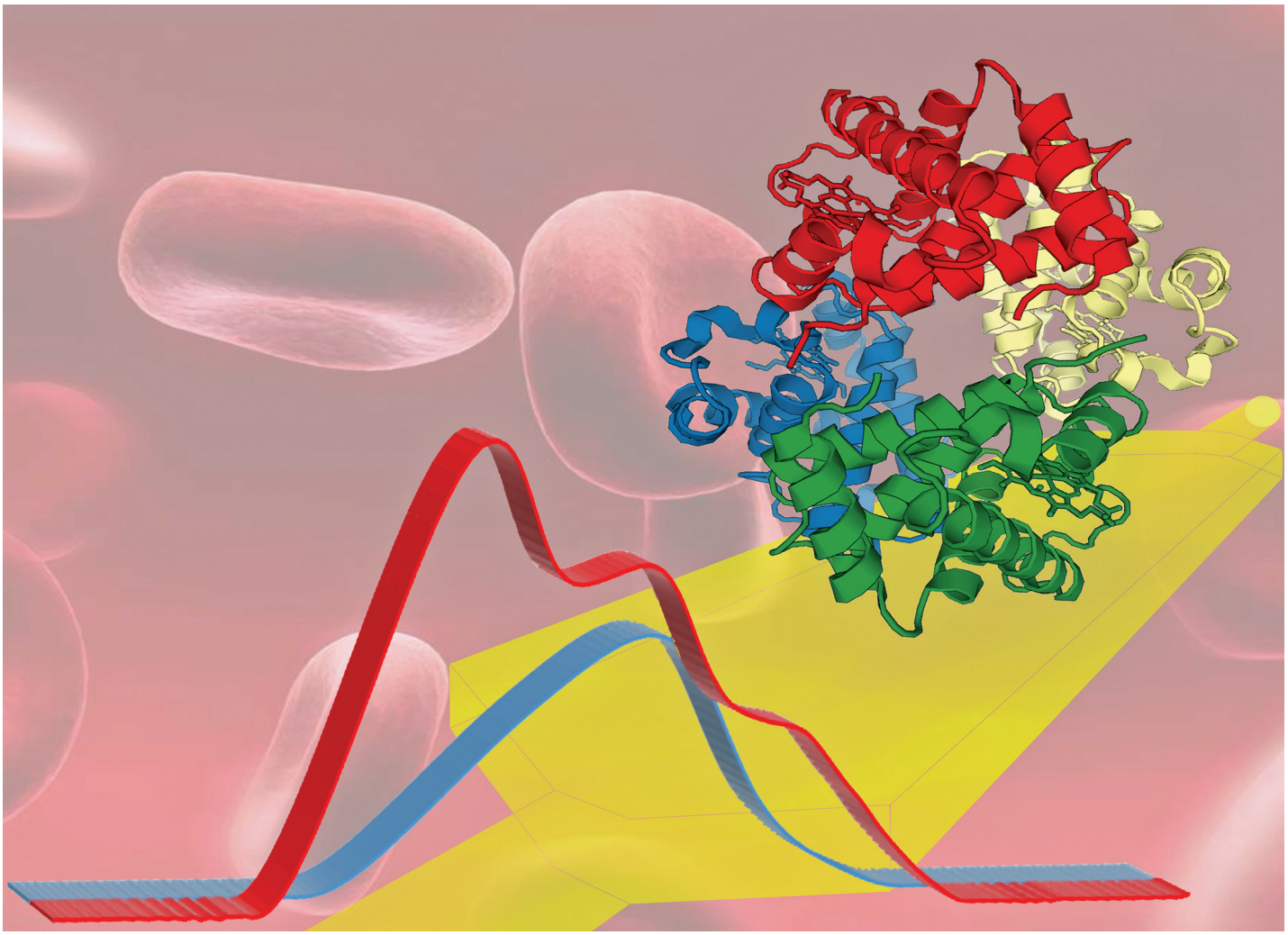

Showcasing collaborative research by Ulm University, Germany, Tel-Aviv University and Ariel University, Israel, and Nanjing University of Science and Technology and University of Science and Technology, China.

Fourier transform infrared spectroscopy on external perturbations inducing secondary structure changes of hemoglobin

The secondary structure changes of hemoglobin during heating is investigated *via* infrared attenuated total reflection spectroscopy using planar silver halide fibers as waveguide. Secondary derivatives, curve fitting, and two-dimensional correlation spectroscopy are applied to reveal secondary structure and conformation information.

As featured in:

See Boris Mizaikoff, Han-Qing Yu *et al.*, *Analyst*, 2016, **141**, 6061.

ROYAL SOCIETY OF CHEMISTRY

www.rsc.org/analyst

Registered charity number: 207890

Analyst

PAPER

View Article Online
View Journal | View Issue

Cite this: *Analyst*, 2016, **141**, 6061

Fourier transform infrared spectroscopy on external perturbations inducing secondary structure changes of hemoglobin†

Rui Lu,[a,b] Wen-Wei Li,[b] Abraham Katzir,[c] Yosef Raichlin,[d] Boris Mizaikoff*[e] and Han-Qing Yu*[b]

Received 29th June 2016,
Accepted 8th September 2016

DOI: 10.1039/c6an01477a

www.rsc.org/analyst

The secondary structure of proteins and their conformation are intimately related to their biological functions. In this study, heat-induced changes in the secondary structure and conformation of hemoglobin were investigated *via* infrared attenuated total reflection (IR-ATR) spectroscopy. The secondary structure changes of hemoglobin were derived from IR-ATR spectra using second derivatives and curve fitting. Thereby, the thermal denaturation temperature ranges and the secondary structure changes with temperature were revealed. More detailed information on the secondary structure and conformation was elucidated *via* two-dimensional infrared correlation spectroscopy. This study deciphers the detailed conformational behavior of hemoglobin molecular changes along with temperature, and creates a general methodological framework for analyzing the heat-induced behavior of biomacromolecules.

Introduction

Proteins are biomacromolecules critically involved in almost all biological functions of living organisms. Many proteins – especially those in blood and plasma – may dominantly interact with metal ions,[1,2] viruses,[3] artificial drugs,[4] and medication.[5] The functions of most proteins are intimately related to their three-dimensional structure,[6–9] which could be subjected to a wide variety of non-covalent interactions including electrostatic forces, hydrophobic/hydrophilic effects, van der Waals interactions, and hydrogen bonds.[10–12] As a consequence, the conformational changes of proteins usually lead to – wanted or unwanted – corresponding property changes, including but not limited to assembly, aggregation, amyloid formation, transport, functional changes, and potentially even cause cytotoxicity.[7]

Given the importance of protein conformation in governing their properties, the kinetics and thermodynamics of protein folding/unfolding have been extensively studied in the past few decades towards more advanced molecular diagnostics.[8,13–17] For example, it has been found that many diseases such as amyloid disease, Alzheimer's disease, and Parkinson's disease[18–20] are likely associated with misfolding or aggregation of proteins. Therefore, it is essential to not only elucidate the secondary structure stability but also the dynamic structural properties of proteins.

Hemoglobin is an important respiratory protein in red blood cells, being critically involved in oxygen transport and electron transfer processes,[21] existing as a tetrameric blood protein composed of two α- and two β-subunits,[22] and capable of binding to various exogenous and endogenous agents.[23] Thus, hemoglobin is considered an ideal model for the investigation of protein properties and structure–function relationships.[24–26]

Therefore, in the present study we have used hemoglobin as a model protein to investigate its denaturation processes and secondary structure changes with temperature. We have adopted a measurement strategy based on the principles of infrared attenuated total reflection (IR-ATR) *via* Fourier transform infrared (FTIR) spectroscopy. While we have fundamentally shown in a previous study that this approach is feasible, we now demonstrate that this strategy is indeed generally applicable,[27] *i.e.*, similar to conventional methods for characterizing protein conformational changes.[28–31] With the concerted application of IR-ATR spectroscopy, second

[a]*Jiangsu Key Laboratory of Chemical Pollution Control and Resources Reuse, School of Environmental and Biological Engineering, Nanjing University of Science and Technology, Nanjing, 210094, China*
[b]*CAS Key Laboratory of Urban Pollutant Conversion, Department of Chemistry, University of Science and Technology of China, Hefei 230026, P.R. China. E-mail: hqyu@ustc.edu.cn*
[c]*School of Physics, Tel-Aviv University, Tel-Aviv 69978, Israel*
[d]*Department of Applied Physics, Ariel University Center of Samaria, Ariel, Israel*
[e]*Institute of Analytical and Bioanalytical Chemistry, Ulm University, 89081 Ulm, Germany. E-mail: boris.mizaikoff@uni-ulm.de*
†Electronic supplementary information (ESI) available. See DOI: 10.1039/c6an01477a

derivatives, appropriate curve fitting methods, and optimized band assignments, we have elucidated the secondary structure changes of hemoglobin by using temperature as the external perturbation. Furthermore, we have used two-dimensional (2D) infrared correlation spectroscopy[32–34] to reveal more detailed information on temperature-induced structural rearrangements of hemoglobin.

Experimental

Chemicals

Hemoglobin from bovine blood (CAS number: 9008-02-0) was purchased from Sigma Co., USA, and was used without further purification. Prior to the experiments, bovine hemoglobin (BHb) was dissolved in D_2O to a final concentration of 0.5%, and kept for 2 days. Here, D_2O instead of H_2O was used in order to avoid strong H–O absorptions within the amide I spectral regime, while preserving the protein peak position.[35,36]

Instrumentation

IR-ATR spectra were obtained *via* a FTIR spectrometer equipped with a mercury–cadmium–telluride (MCT) semiconductor detector cooled with liquid nitrogen (Vector 22, Bruker Optics, Ettlingen, Germany). A planar silver halide fiber segment was adapted for ATR sensing using minute sample volumes (*i.e.*, 5 ml). Cylindrical silver halide fibers were fabricated by hot extrusion from a single crystal preform, which was prepared using the well-established Bridgman–Stockbarger technique. After preparing short fiber segments (length approx. 100 mm) by cutting, a planar section was fabricated *via* a stainless-steel mold by pressing a short cylindrical fiber section into a planar geometry tapering into cylindrical in- and out-coupling segments. The fiber was sealed into a flow cell equipped with a heating system for temperature control. The fiber ATR sensing element comprises cylindrical segments at both ends facilitating radiation in-/out-coupling with a planar active sensing segment as the middle section (Fig. 1). Such a unique geometry ensures an increased number of internal reflections, and hence, superior detection sensitivity compared to cylindrical fibers and conventional multi-reflection ATR crystals.[27,37–39] Prior to the measurement, each sample was equilibrated for at least 5 min after reaching the targeted temperature. Then, a total of 64 spectral scans were averaged at a spectral resolution of 2 cm^{-1} in a frequency window of 4000 to 400 cm^{-1}. Thus, a series of spectra of protein samples at temperatures from 26 (*i.e.*, room temperature) to 90 °C at 2 °C intervals was obtained. Each experiment was performed at least in duplicate. Although the current fabrication procedure of flat-tapered fibers usually yields variations in transducer thickness, for each fiber an individual background spectrum was recorded. Thereby, self-consistent and comparable results were obtained ensuring comparability despite fiber-to-fiber variations. It is anticipated that such fiber optic transducer segments will be a readily replaceable and cheap consumable during extended studies.

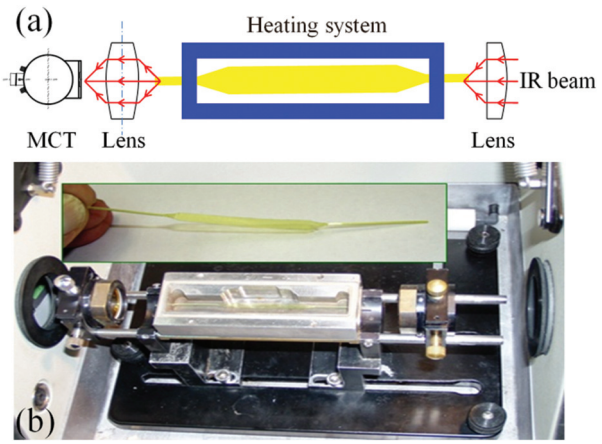

Fig. 1 Custom-made fiber optic sensing arrangement using a planar-tapered silver halide fiber segment (see inset for details) housed in a flow cell equipped with a heating system optically coupled to the FTIR spectrometer. (a) Schematic experimental set-up, and (b) the image of the sensing arrangement comprising the planarized silver halide fiber.

Data processing

The obtained spectral data were processed using the OPUS 5.5 software (Bruker Optics, Ettlingen, Germany). First, in the amide I range (*i.e.*, 1600–1700 cm^{-1}) the spectra were region-selected and baseline corrected. Then, the spectra were processed by calculating second derivatives, and the obtained peaks were fitted using Gaussians. During the fitting process, parameters including the height, width, and frequency position of all bands were adjusted with the initial values given by the peaks of the calculated second derivatives.

2D correlation spectroscopy

Two-dimensional (2D) correlation spectroscopy was initially dominated by nuclear magnetic resonance (NMR) and other resonance spectroscopy methods. Later, Noda has seminally proposed a different approach, *i.e.*, applying perturbation-based 2D spectroscopy to infrared spectroscopy (2D-IR).[40] Since then, this technique has found applications in many research areas. 2D spectroscopy consists of two orthogonal components, the synchronous and asynchronous correlation spectra. Among the important characteristics of 2D spectroscopy is that both synchronous and asynchronous correlation spectra contain distinct and useful information for subsequent analysis. In the present study, 2D correlation spectroscopy was advantageously used to probing the BHb secondary structure specific 'sequential order', which is based on the changes of infrared spectral intensity during the heating process. Matlab R2012a (Mathworks Inc., USA) was used for all associated 2D spectral calculations.

Results and discussion

Infrared spectra in the amide I range (1600–1700 cm^{-1}) during heating from 26 °C (room temperature) to 90 °C were collected, smoothed, and baseline corrected.

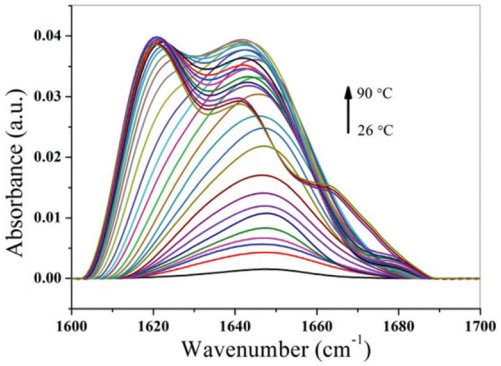

Fig. 2 IR-ATR spectra of BHb in D_2O in the temperature range of 26–90 °C at 2 °C temperature intervals after smoothing and baseline correction.

Fig. 2 shows that the protein spectra, *i.e.*, the amide-I vibration arose with increasing temperature with main contributions by the C═O stretching vibration next to the NH in-plane bending, the out-of-phase CN stretching, and the CCN deformation vibration.[41] This result was ascribed to the peptide backbone carbonyl stretching vibrations that are governed by the interaction between the amide units and the hydrogen bond,[42] while the side chain apparently had almost no effect on the amide-I vibration. Given its dependence predominantly on the backbone secondary structure, the amide-I absorption may thus be used for a detailed secondary structure analysis.[41] It is critical to assign the individual contributions to the amide-I band region by different elements of the BHb secondary structure. For most proteins, the bands at 1618–1623 cm^{-1}, 1618–1642 cm^{-1}, 1651–1658 cm^{-1}, 1666–1688 cm^{-1}, and 1683–1689 cm^{-1} may be ascribed to intermolecular aggregates, β-sheets, α-helix, turns, and intramolecular aggregates, respectively.[42–45] More detailed characteristic curves are shown in the ESI.†

To further obtain peak position information, we have processed the spectra shown in Fig. 2 by calculating derivatives. Several characteristic second derivatives spectra were obtained at 26, 42, 60, 84, and 86 °C, respectively (Fig. 3). In these spectra, the peak positions representative of the corresponding bands were used for further curve fitting.[27] At 26 °C, only one peak evolved at 1648 cm^{-1}. When increasing the temperature to 42 °C, an additional peak at 1626 cm^{-1} appeared. At 60 °C, the peak at 1648 cm^{-1} shifted to 1646 cm^{-1}, while the one at 1626 cm^{-1} shifted to 1620 cm^{-1}. Once the temperature reached 84 °C, the peak at 1646 cm^{-1} remained at that frequency position, while the one at 1620 cm^{-1} shifted to 1618 cm^{-1}, and a new peak emerged at 1680 cm^{-1}. When further increasing the temperature to 86 °C, the peak at 1646 cm^{-1} shifted to 1642 cm^{-1}, while the one at 1618 cm^{-1} remained at that wavelength. The most evident changes were that the peak at 1680 cm^{-1} disappeared, while a new peak appeared at 1666 cm^{-1}.

After curve fitting (details given in ESI Fig. 4–7†), the deconvoluted amide-I band information along with the temperature trace was obtained (Fig. 4). Typically, either Lorentzian, Gaussian, or a combination of these two peak shapes are used to describe the contributions within the amide-I band.[46] In the present study, deconvolution into Gaussians provided the best curve fitting results.[47] As each peak then corresponds to a particular BHb secondary structure element, appropriate band assignment should enable assigning the associated secondary structure changes during heat treatment of BHb.

In general, the 1620 cm^{-1} band is ascribed to intermolecular aggregate, while the 1678 cm^{-1} band is associated with intramolecular aggregates.[42,47,48] In both the intermolecular and intramolecular aggregates, hydrogen bonds readily establish with the polypeptide strands, *i.e.*, the C═O and N–H moieties. Thus, hydrogen bonds may be associated with intermolecular and intramolecular interactions giving rise to stable aggregates.[48]

Here, the 1626 cm^{-1} band was assigned to the BHb β-sheet structure for several reasons. Usually, antiparallel β-sheets give rise to two bands in the amide-I region, *i.e.*, one strong band at 1630 cm^{-1}, and one relatively weak band at 1685 cm^{-1}. The band position may be affected by the number of strands, rather than by the number of amide groups within the strands. Thus, if the β-sheet structure has a larger number of strands,

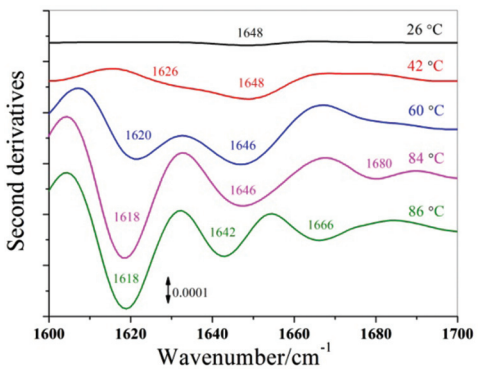

Fig. 3 Second derivatives of the BHb IR-ATR spectra at 26, 42, 60, 84, and 86 °C.

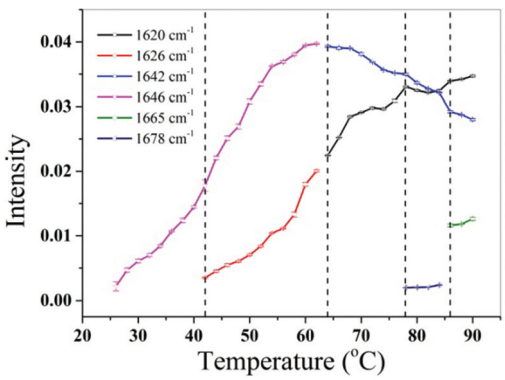

Fig. 4 Evaluated selected peak intensities represented as a function of applied temperature.

the spectral shift of the main band would occur towards lower wavenumbers.[49–51] Another factor affecting the band position is twisting, which could decrease the splitting between the low and high bands. Furthermore, twisting can also initiate a shift of the main band towards higher wavenumbers, *i.e.*, towards the antiparallel β-sheet. However, the twisting effect is considered relatively minute for parallel β-sheets.[52] While the parallel β-sheet band[49,53] may shift to 1619 cm^{-1} for some peptides in D_2O,[54] the difference between parallel β-sheets and antiparallel β-sheets could be as small as 4 cm^{-1}.[54] Compared to the antiparallel β-sheet, the parallel β-sheet predominantly occurs at higher wavenumbers.[51,53] Another difference between the parallel β-sheet and the antiparallel β-sheet is that the former has a smaller splitting between main and side bands. Last but not least, the high wavenumber side band of the parallel β-sheet structure is less intense.[49,51] Thus, the high wavenumber component of parallel β-sheet structures is occasionally absent in the corresponding IR spectra.[54–56] However, when comparing parallel β-sheets with several strands with twisted or few strands of antiparallel β-sheets, the difference becomes unnoticeable.[49,51,52] Thus, it is increasingly difficult to distinguish these two β-sheet structures within proteins only *via* experimental results and in the absence of extensive structural dynamics modeling.[55,57,58] Consequently, herein the 1626 cm^{-1} band was assigned to β-sheets without further discrimination between parallel and antiparallel units.

Folded proteins are characterized by a structured amide-I spectrum, while the unfolded protein exhibits a broad yet featureless band around 1650 cm^{-1}.[59–62] Thus, the 1642 cm^{-1} band should be ascribed to unordered structures. Also, the 1642 cm^{-1} band appeared only at relatively high temperatures (*i.e.*, 64 °C in the present experiments shown in Fig. 4), thus further supporting the assignment of the feature at 1642 cm^{-1} to unordered structures.

The band at 1646 cm^{-1} was readily assigned to α-helix structures within BHb. Previous experimental and computational studies have established some rules of thumb describing how the amide-I IR absorption is affected by the backbone structure. Usually, the α-helix has two absorption bands; the main band close to 1655 cm^{-1}, and a shoulder band at lower wavenumbers.[57,63] However, the main band position may shift towards lower wavenumbers, if some internal properties of the protein or the external environment change, for example an extended helix length,[63] a bent in coiled segments,[64,65] or exposure to different solvents. In D_2O, the absorption maximum appears at approx. 1629–1640 cm^{-1}, while in H_2O the maximum is observed at 1640–1650 cm^{-1}.[66–69] Therefore, the 1646 cm^{-1} band should readily correspond to the BHb α-helix in the present experiments.

Finally, the band at 1665 cm^{-1} should be ascribed to the vibrational modes of β-turns within the protein secondary structure.[41,42,48,56,70] The derived band assignments for the BHb secondary structure elements are summarized in Table 1.

At the initial temperature of 26 °C, only one peak at 1646 cm^{-1} was observed, thereby indicating the presence of the α-helix. With an increase in temperature to 42 °C, a peak appeared at 1626 cm^{-1} suggesting that β-sheet structures are established at this temperature. At 64 °C, the peaks at 1646 cm^{-1} and 1626 cm^{-1} both disappeared, while two new peaks appeared at 1642 cm^{-1} and 1620 cm^{-1}. This result indicates that both α-helix and β-sheet structures were affected by the temperature change leading to the formation of unordered and intermolecular aggregates. Thus, it may be inferred that the ordered secondary structures are less stable during extensive environmental perturbations, and that unordered structures, including hydrogen bonds formed in both intermolecular and intramolecular aggregates, remain stable at relatively high temperatures. This is furthermore confirmed by the fact that both the peaks at 1642 and at 1620 cm^{-1}, which represent unordered and intermolecular aggregates, respectively, existed until the highest temperature was reached at the end of the experiment. Besides, at 78 °C a new peak appeared at 1678 cm^{-1} indicating the formation of intramolecular aggregates. At 86 °C, the 1665 cm^{-1} peak, which represents β-turn structures, was apparent. Compared to previous studies,[71] temperatures from 30–44 °C were suggested as the initial structural perturbation stage, which is consistent with our result indicating that the first structural change occurred at 42 °C. It was also shown that at temperatures below 44 °C the structure was dominated by the α-helix and extended chain structure changes,[71] while our results revealed that 42 °C was a temperature specifically conducive to α-helices. The temperature range between 46 and 60 °C for the α-helix was herein determined rather from 42 to 62 °C. According to the literature,[71] temperatures above 62 °C caused α-helix and intermolecular β-sheet changes; in comparison, our results confirm that α-helices and β-sheets are dramatically altered when exceeding 64 °C. As experiments beyond 70 °C were not reported, no further results were available for comparison at elevated temperatures. In summary, the results reported herein are highly consistent with previously published research; likewise, previous studies of our research team using similar sensing concepts yet for other proteins have confirmed consistency of the obtained results with previously published data.[27] Thus, it may be stated that the analytical procedure based on the IR-ATR spectra shown herein facilitates mapping the entire process of secondary structure changes within the BHb protein in response to an external perturbation, *i.e.*, here, temperature. It should be noted that a contribution to the increase in infrared absorbance next to temperature may also be resulting from an

Table 1 Frequency position and assignments of IR bands associated with BHb secondary structure elements in D_2O

Wavenumber (cm^{-1})	Assignment (BHb secondary structure element)
1678	Intramolecular aggregate
1665	β-Turn
1646	α-Helix
1642	Unordered
1626	β-Sheet
1620	Intermolecular aggregate

increased BHb concentration, *e.g.*, *via* accumulation within the evanescent field.

Even more detailed information on the secondary structure change sequence may be revealed *via* the associated 2D correlation spectra. As the temperature was increased from minimum (T_{min}) to maximum (T_{max}) during the experiments, the overall similarity or coincidental trends between two separate intensity variations in the 2D correlation spectra are encoded in the synchronous intensity $\Phi(\nu_1, \nu_2)$, while the dissimilarity or out-of-phase character of the spectral intensity variations is reflected by the asynchronous intensity $\Psi(\nu_1, \nu_2)$.[40]

In the synchronous spectrum, some 'diagonal peaks' can be observed, which are referred to as 'autopeaks'. These autopeaks correspond to the autocorrelation function of the spectral intensity variations observed during the external disturbance intervals T_{min} and T_{max}. Also, at any given perturbation (here, temperature changes), if the intensity changes dominate in any region of the synchronous spectrum, a strong autopeak would appear. Correspondingly, if the intensity remains nearly constant, only a small or no autopeak would be observed.

In the asynchronous spectrum, there is no autopeak observed, yet, so-called 'cross peaks' may only be located at off-diagonal positions. The cross peaks only exist if two spectral feature intensities change out of phase from each other. This property is especially useful for discriminating different secondary structure elements with overlapping spectral bands. To explain this in detail, some examples are given in the following. Heterogeneous materials containing, *e.g.*, multiple phases or regions/domains, a complex mixture comprising individual components with different spectral intensities or chemical functional groups with different responses to an external perturbation could be effectively discriminated. As long as the sequential variations of the spectral intensities along the external perturbation are different, the cross peaks will appear in between their spectral coordinates in the asynchronous spectrum, even if the spectral bands are closely located from each other.

Similar to the synchronous spectrum, the signs of the cross peaks in the asynchronous spectrum are either positive or negative. This provides information on the 'sequential order' of events along the external perturbation. According to Noda's rules,[40] if $\Phi(\nu_1, \nu_2) > 0$, $\Psi(\nu_1, \nu_2) > 0$, the ν_1 intensity change would occur predominantly 'before' ν_2 in the 'sequential order', if time is the external perturbation. However, if $\Phi(\nu_1, \nu_2) < 0$, $\Psi(\nu_1, \nu_2) > 0$, the ν_1 change would occur predominantly 'after' ν_2, again with time as the external perturbation. The two other situations are exactly the opposite with $\Phi(\nu_1, \nu_2) < 0$. In the present study, as temperature (and not time) is the external perturbation, the 'sequential order' is not appropriately explained with 'before' or 'after'. Thus, one may refer to the associated secondary structure changes as 'easy' or 'hard' according to the external perturbation.

The synchronous and asynchronous correlation spectra are shown in Fig. 5. The signs of the cross peaks are summarized in Table 2. From the synchronous spectrum, the autopeak intensity orders of these three peaks were: 1646 > 1620 > 1678 cm^{-1}. This result indicates that during the temperature perturbation the peak intensity at 1646 cm^{-1} had the largest change while that at 1678 cm^{-1} had the least changes. As discussed above, the peak at 1646 cm^{-1} represents the α-helix, and those at 1620 and 1678 cm^{-1} are associated with intermolecular and intramolecular aggregates, respectively. Thus, it can be concluded that the α-helix undergoes the strongest structure change, while the intermolecular aggregate was subject to a medium change; the intramolecular aggregate was therefore least affected. These results are in fact highly consistent with the results derived from Fig. 4. In combination of the synchronous and asynchronous spectra, the 'sequential orders' of the bands during the perturbation were obtained as 1646 < 1620 cm^{-1}, and 1678 > 1646 cm^{-1}. This indicates that the intermolecular and intramolecular aggregates changed more than the α-helix structure with temperature as the external perturbation. This finding agrees with the fact that both intermolecular and intramolecular aggregate structures are

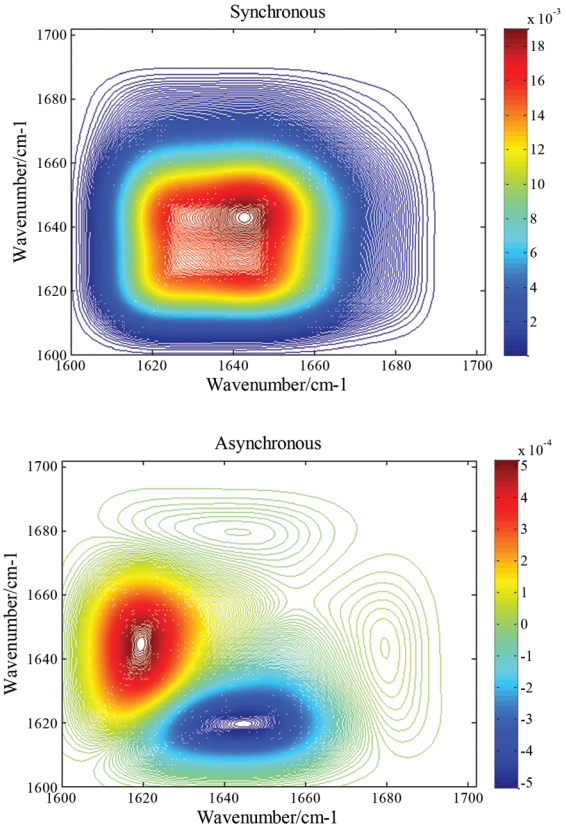

Fig. 5 Synchronous and asynchronous 2D IR correlation spectra of BHb in D_2O with temperature as the external perturbation.

Table 2 Signs of the synchronous (Φ) and asynchronous (Ψ) cross peaks

(ν_1, ν_2)	Φ	Ψ	'Sequential order'
(1646, 1620)	+	−	1646 < 1620
(1678, 1646)	+	+	1678 > 1646

relatively flexible, while the α-helix structure is considered more rigid.

Therefore, it may be concluded that the α-helix structure is rigid and it does not readily change with temperature. However, once the perturbation reaches a critical value (here, 64 °C), the α-helix may not maintain its structural integrity anymore and will be denatured, thereby significantly affecting the infrared spectrum. In contrast, the intermolecular and intramolecular aggregates are prone to structural changes associated with temperature owing to their relatively flexible conformations, accordingly yielding less intensity changes compared to the α-helix.

Conclusions

A heat-induced BHb denaturation process was mapped in detail by IR-ATR spectroscopy, whereby a flat-tapered silver halide fiber serving as a readily replaceable transducer was used as the active sensing element facilitating IR-spectroscopic studies in minute sample volumes. By calculating second derivatives of the obtained IR-ATR spectra along with appropriate curve fitting procedures, the contributions of individual secondary structure elements of the protein to the sum amide-I absorption feature were precisely allocated using the Gaussian peaks. Furthermore, 2D correlation IR spectroscopy revealed more detailed information on BHb secondary structure changes with temperature. Importantly, after fundamental studies on BSA we have now extended this methodology to BHb, thereby demonstrating that the developed strategy is generally applicable, and may be readily adapted as a routine tool to study protein secondary structure changes in molecular detail in response to external perturbations such as temperature, pH, heavy metals, and potentially even adsorption at surfaces.

Acknowledgements

The authors wish to thank the Natural Science Foundation of China (21505074), the Natural Science Foundation of Jiangsu Province (BK20140781), the Fundamental Research Funds for the Central University (no. 30920140112010) and the Priority Academic Program Development of Jiangsu Higher Education Institutions for the partial support of this work.

References

1 L.-Z. Wu, B.-L. Ma, D.-W. Zou, Z.-X. Tie, J. Wang and W. Wang, *J. Mol. Struct.*, 2008, **877**, 44–49.
2 B. Gong, Y. Chen, E. L. Christian, J.-H. Chen, E. Chase, D. M. Chadalavada, R. Yajima, B. L. Golden, P. C. Bevilacqua and P. R. Carey, *J. Am. Chem. Soc.*, 2008, **130**, 9670–9672.
3 M. A. Calderwood, K. Venkatesan, L. Xing, M. R. Chase, A. Vazquez, A. M. Holthaus, A. E. Ewence, N. Li, T. Hirozane-Kishikawa and D. E. Hill, *Proc. Natl. Acad. Sci. U. S. A.*, 2007, **104**, 7606–7611.
4 A. Taubert, *Proc. Natl. Acad. Sci. U. S. A.*, 2007, **104**, 20643–20644.
5 J. Tian, J. Liu, J. Zhang, Z. Hu and X. Chen, *Chem. Pharm. Bull.*, 2003, **51**, 579–582.
6 C. M. Dobson, *Nature*, 2003, **426**, 884–890.
7 H.-W. He, J. Zhang, H.-M. Zhou and Y.-B. Yan, *Biophys. J.*, 2005, **89**, 2650–2658.
8 X. Li, W. Zheng, L. Zhang, P. Yu, Y. Lin, L. Su and L. Mao, *Anal. Chem.*, 2009, **81**, 8557–8563.
9 Q. Wang, W. Xu, P. Wu, H. Zhang, C. Cai and B. Zhao, *J. Phys. Chem. B*, 2010, **114**, 12754–12764.
10 A. Ahmad, M. S. Akhtar and V. Bhakuni, *Biochemistry*, 2001, **40**, 1945–1955.
11 M. D. Gouda, S. A. Singh, A. G. A. Rao, M. S. Thakur and N. G. Karanth, *J. Biol. Chem.*, 2003, **278**, 24324–24333.
12 D. Perl, U. Mueller, U. Heinemann and F. X. Schmid, *Nat. Struct. Mol. Biol.*, 2000, **7**, 380–383.
13 E. Botello, N. C. Harris, J. Sargent, W.-H. Chen, K.-J. Lin and C.-H. Kiang, *J. Phys. Chem. B*, 2009, **113**, 10845–10848.
14 E. Saguer, P. Alvarez, J. Sedman, H. S. Ramaswamy and A. A. Ismail, *Food Hydrocolloids*, 2009, **23**, 874–879.
15 Z. Mai, X. Zhao, Z. Dai and X. Zou, *J. Phys. Chem. B*, 2010, **114**, 7090–7097.
16 K. P. Fears, B. Sivaraman, G. L. Powell, Y. Wu and R. A. Latour, *Langmuir*, 2009, **25**, 9319–9327.
17 A. Panuszko, P. Bruździak, J. Zielkiewicz, D. Wyrzykowski and J. Stangret, *J. Phys. Chem. B*, 2009, **113**, 14797–14809.
18 R. J. Ellis and T. J. T. Pinheiro, *Nature*, 2002, **416**, 483–484.
19 M. R. Sawaya, S. Sambashivan, R. Nelson, M. I. Ivanova, S. A. Sievers, M. I. Apostol, M. J. Thompson, M. Balbirnie, J. J. W. Wiltzius, H. T. McFarlane, A. O. Madsen, C. Riekel and D. Eisenberg, *Nature*, 2007, **447**, 453–457.
20 A. Baumketner, M. G. Krone and J.-E. Shea, *Proc. Natl. Acad. Sci. U. S. A.*, 2008, **105**, 6027–6032.
21 A. K. Sau, D. Currell, S. Mazumdar and S. Mitra, *Biophys. Chem.*, 2002, **98**, 267–273.
22 Y. Yuan, V. Simplaceanu, J. A. Lukin and C. Ho, *J. Mol. Biol.*, 2002, **321**, 863–878.
23 T. Yonetani and M. Laberge, *Biochim. Biophys. Acta, Proteins Proteomics*, 2008, **1784**, 1146–1158.
24 J. Choi and M. Terazima, *J. Phys. Chem. B*, 2002, **106**, 6587–6593.
25 L. B. Sagle, J. Zimmermann, P. E. Dawson and F. E. Romesberg, *J. Am. Chem. Soc.*, 2004, **126**, 3384–3385.
26 V. L. Robinson, B. B. Smith and A. Arnone, *Biochemistry*, 2003, **42**, 10113–10125.
27 R. Lu, W.-W. Li, A. Katzir, Y. Raichlin, H.-Q. Yu and B. Mizaikoff, *Analyst*, 2014, **140**, 765–770.
28 X. Hu, D. Kaplan and P. Cebe, *Macromolecules*, 2008, **41**, 3939–3948.
29 E. Sherman, A. Itkin, Y. Y. Kuttner, E. Rhoades, D. Amir, E. Haas and G. Haran, *Biophys. J.*, 2008, **94**, 4819–4827.
30 F. Wang, J. Wang, X. Liu and S. Dong, *Talanta*, 2008, **77**, 628–634.

31 S. Baird, S. M. Kelly, N. C. Price, E. Jaenicke, C. Meesters, D. Nillius, H. Decker and J. Nairn, *Biochim. Biophys. Acta, Proteins Proteomics*, 2007, **1774**, 1380–1394.
32 C. P. Schultz, O. Bârzu and H. H. Mantsch, *Appl. Spectrosc.*, 2000, **54**, 931–938.
33 I. Noda, A. E. Dowrey, C. Marcoli, G. M. Story and Y. Ozaki, *Appl. Spectrosc.*, 2000, **54**, 236A–248A.
34 Y. M. Jung, B. Czarnik-Matusewicz and Y. Ozaki, *J. Phys. Chem. B*, 2000, **104**, 7812–7817.
35 D. Neubauer, J. Korbmacher, M. Frick, J. Kiss, M. Timmler, P. Dietl, O. H. Wittekindt and B. Mizaikoff, *Anal. Chem.*, 2013, **85**, 4247–4250.
36 J. P. Korbmacher, C. Michel, D. Neubauer, K. Thompson, B. Mizaikoff, M. Frick, P. Dietl and O. H. Wittekindt, *Physiol. Rep.*, 2014, **2**, e00201.
37 R. Lu, W.-W. Li, B. Mizaikoff, A. Katzir, Y. Raichlin, G.-P. Sheng and H.-Q. Yu, *Nat. Protocols*, 2016, **11**, 377–386.
38 R. Lu, G. Sheng, W. Li, H. Yu, Y. Raichlin, A. Katzir and B. Mizaikoff, *Angew. Chem., Int. Ed.*, 2013, **52**, 2265–2268.
39 R. Lu, B. Mizaikoff, W.-W. Li, C. Qian, A. Katzir, Y. Raichlin, G.-P. Sheng and H.-Q. Yu, *Sci. Rep.*, 2013, **3**, 2525–2530.
40 I. Noda and Y. Ozaki, *Two-dimensional correlation spectroscopy: applications in vibrational and optical spectroscopy*, John Wiley & Sons, 2005.
41 A. Barth, *Biochim. Biophys. Acta, Bioenerg.*, 2007, **1767**, 1073–1101.
42 P. Pal, T. Kamilya, M. Mahato and G. B. Talapatra, *Colloids Surf., B*, 2009, **73**, 122–131.
43 N. Brandes, P. B. Welzel, C. Werner and L. W. Kroh, *J. Colloid Interface Sci.*, 2006, **299**, 56–69.
44 M. Mahato, P. Pal, T. Kamilya, R. Sarkar and G. B. Talapatra, *J. Phys. Chem. B*, 2010, **114**, 495–502.
45 L. Shang, Y. Wang, J. Jiang and S. Dong, *Langmuir*, 2007, **23**, 2714–2721.
46 T. Kamilya, P. Pal, M. Mahato and G. B. Talapatra, *J. Phys. Chem. B*, 2009, **113**, 5128–5135.
47 M. Mahato, P. Pal, T. Kamilya, R. Sarkar, A. Chaudhuri and G. B. Talapatra, *J. Phys. Chem. B*, 2010, **114**, 7062–7070.
48 L. Dziri, B. Desbat and R. M. Leblanc, *J. Am. Chem. Soc.*, 1999, **121**, 9618–9625.
49 Y. N. Chirgadze and N. A. Nevskaya, *Biopolymers*, 1976, **15**, 627–636.
50 J. Kubelka and T. A. Keiderling, *J. Am. Chem. Soc.*, 2001, **123**, 6142–6150.
51 Y. N. Chirgadze and N. A. Nevskaya, *Biopolymers*, 1976, **15**, 607–625.
52 J. Kubelka and T. A. Keiderling, *J. Am. Chem. Soc.*, 2001, **123**, 12048–12058.
53 S. Krimm and Y. Abe, *Proc. Natl. Acad. Sci. U. S. A.*, 1972, **69**, 2788–2792.
54 P. Chitnumsub, W. R. Fiori, H. A. Lashuel, H. Diaz and J. W. Kelly, *Bioorg. Med. Chem.*, 1999, **7**, 39–59.
55 R. Khurana and A. L. Fink, *Biophys. J.*, 2000, **78**, 994–1000.
56 N. Yamada, K. Ariga, M. Naito, K. Matsubara and E. Koyama, *J. Am. Chem. Soc.*, 1998, **120**, 12192–12199.
57 H. Torii and M. Tasumi, *J. Chem. Phys.*, 1992, **96**, 3379–3387.
58 H. Susi and D. M. Byler, *Arch. Biochem. Biophys.*, 1987, **258**, 465–469.
59 W. K. Surewicz, J. J. Leddy and H. H. Mantsch, *Biochemistry*, 1990, **29**, 8106–8111.
60 M. Jackson, P. I. Haris and D. Chapman, *Biochemistry*, 1991, **30**, 9681–9686.
61 J. L. R. Arrondo and F. M. Goñi, *Prog. Biophys. Mol. Biol.*, 1999, **72**, 367–405.
62 M. Jackson and H. H. Mantsch, *Biochim. Biophys. Acta, Protein Struct. Mol. Enzymol.*, 1991, **1078**, 231–235.
63 N. A. Nevskaya and Y. N. Chirgadze, *Biopolymers*, 1976, **15**, 637–648.
64 W. C. Reisdorf and S. Krimm, *Biochemistry*, 1996, **35**, 1383–1386.
65 T. Heimburg, J. Schuenemann, K. Weber and N. Geisler, *Biochemistry*, 1996, **35**, 1375–1382.
66 S. Y. Venyaminov and N. N. Kalnin, *Biopolymers*, 1990, **30**, 1259–1271.
67 Y. N. Chirgadze and E. Brazhnikov, *Biopolymers*, 1974, **13**, 1701–1712.
68 G. Martinez and G. Millhauser, *J. Struct. Biol.*, 1995, **114**, 23–27.
69 S. Mukherjee, P. Chowdhury and F. Gai, *J. Phys. Chem. B*, 2007, **111**, 4596–4602.
70 T. Kamilya, P. Pal and G. B. Talapatra, *Biophys. Chem.*, 2010, **146**, 85–91.
71 Y. B. Yan, Q. Wang, H. W. He and H. M. Zhou, *Biophys. J.*, 2004, **86**, 1682–1690.